Temporally Irregular Mnemonic Persistent Activity in Prefrontal Neurons of Monkeys During a Delayed Response Task

Albert Compte,[1,2] Christos Constantinidis,[3] Jesper Tegnér,[1,4,5] Sridhar Raghavachari,[1] Matthew V. Chafee,[3] Patricia S. Goldman-Rakic,[3] and Xiao-Jing Wang[1]

[1]*Volen Center for Complex Systems, Brandeis University, Waltham, Massachusetts 02454;* [2]*Instituto de Neurociencias, Universidad Miguel Hernández-Consejo Superior de Investigaciones Científicas, 03550 San Juan de Alicante, Spain;* [3]*Section of Neurobiology, Yale School of Medicine, New Haven, Connecticut 06520;* [4]*Stockholm Bioinformatic Center, SCFAB, S-10691 Stockholm; and* [5]*Computational Biology, Department of Physics, Linköpings Institute of Technology, S-581 83 Linköping, Sweden*

Compte, Albert, Christos Constantinidis, Jesper Tegnér, Sridhar Raghavachari, Matthew V. Chafee, Patricia S. Goldman-Rakic, and Xiao-Jing Wang. Temporally irregular mnemonic persistent activity in prefrontal neurons of monkeys during a delayed response task. *J Neurophysiol* 90: 3441–3454, 2003. First published May 28, 2003; 10.1152/jn.00949.2002. An important question in neuroscience is whether and how temporal patterns and fluctuations in neuronal spike trains contribute to information processing in the cortex. We have addressed this issue in the memory-related circuits of the prefrontal cortex by analyzing spike trains from a database of 229 neurons recorded in the dorsolateral prefrontal cortex of 4 macaque monkeys during the performance of an oculomotor delayed-response task. For each task epoch, we have estimated their power spectrum together with interspike interval histograms and autocorrelograms. We find that *1*) the properties of most (about 60%) neurons approximated the characteristics of a Poisson process. For about 25% of cells, with characteristics typical of interneurons, the power spectrum showed a trough at low frequencies (<20 Hz) and the autocorrelogram a dip near zero time lag. About 15% of neurons had a peak at <20 Hz in the power spectrum, associated with the burstiness of the spike train; *2*) a small but significant task dependency of spike-train temporal structure: delay responses to preferred locations were characterized not only by elevated firing, but also by suppressed power at low (<20 Hz) frequencies; and *3*) the variability of interspike intervals is typically higher during the mnemonic delay period than during the fixation period, regardless of the remembered cue. The high irregularity of neural persistent activity during the delay period is likely to be a characteristic signature of recurrent prefrontal network dynamics underlying working memory.

INTRODUCTION

The ability to hold and manipulate information in memory for short periods of time has been termed *working memory* and constitutes a crucial element of higher cognitive functions. Imaging techniques in humans (Courtney et al. 1997; Jonides et al. 1993; Leung et al. 2002; McCarthy et al. 1994) and electrophysiological experiments in monkeys (Funahashi et al. 1989; Fuster and Alexander 1971; Kubota and Niki 1971) have identified the prefrontal cortex as an area critically involved in working memory. A significant proportion of prefrontal neu-

rons show firing rates that are tuned to the position or identity of a sensory stimulus and maintain this tuning persistently across the delay period of a working-memory task, when the stimulus is no longer available to the senses. This tuned persistent activity is regarded as the neural correlate of working memory (Goldman-Rakic 1987, 1995; Wang 2001).

Most previous neurophysiological studies in monkeys have investigated the effect of different stimuli and their maintenance in memory in terms of changes in the mean discharge rate evoked by these events. However, temporal characteristics of the spike train (e.g., oscillations, interneuronal synchronization, or bursting) could, in principle, convey information about task-related events. Oscillatory discharges in particular have received considerable attention over the last decade as the mediator of such functions as attention, figure-ground segregation, memory maintenance, and conscious awareness (Crick 1994; Singer and Gray 1995; Treisman 1996). Oscillations have been reported in the primary visual cortex of the cat and monkey (Eckhorn et al. 1988; Friedman-Hill et al. 2000; Frien et al. 1994; Gray et al. 1989; Livingstone 1996), whereas other studies have contested their prevalence and significance (Ghose and Freeman 1992; Kiper et al. 1996; Young et al. 1992). Fewer studies have examined the existence and possible role of oscillations outside the primary visual cortex, also with conflicting positive (Fries et al. 2001; Kreiter and Singer 1996) and negative (Bair et al. 1994; Cardoso de Oliveira et al. 1997; Tovee and Rolls 1992) results. Notice, however, that positive results are usually observed in population measures like multiunit recordings or local field potentials, whereas single unit activity typically shows little oscillatory behavior. It is conceivable that temporal properties not observed at the neuronal level could emerge from the population collective dynamics (Brunel 2000; Brunel and Wang 2003; Csicsvari et al. 1999).

Recently there are reports suggesting that oscillatory firing may be especially significant in neuronal discharges associated with active memory maintenance in delayed response tasks, compared with baseline spontaneous activity (Pesaran et al. 2002; Tallon-Baudry et al. 2001). Persistent activity during the memory period is believed to be sustained by reverberatory

---

Address for reprint requests and other correspondence: A. Compte, Instituto de Neurociencias, Universidad Miguel Hernández-CSIC, 03550 San Juan de Alicante, Spain (E-mail: acompte@umh.es).

dynamics in a recurrent network (Amit and Brunel 1997; Camperi and Wang 1998; Compte et al. 2000; Durstewitz et al. 2000; Lisman et al. 1998; Wang 1999b, 2001) and it is reasonable to assume that a strongly reverberatory network could promote oscillatory firing under certain conditions, such as when the recurrent excitation is much faster than feedback inhibition (Compte et al. 2000; Tegnér et al. 2002; Wang 1999b). To examine this possibility, we have here applied unbiased analytic methods to investigate the presence of rhythmic activity and its possible correlation with task-related events on a database of neurons recorded in the dorsolateral prefrontal cortex of monkeys as they performed an oculomotor working memory task.

METHODS

Animals

The data used for this study were recorded from 4 male rhesus monkeys (*Macaca mulatta*), weighing 6–12.5 kg. Detailed descriptions of the experimental techniques as well as the firing rate modulations of recorded neurons in terms of their firing rate modulations were published previously (Chafee and Goldman-Rakic 1998; Constantinidis et al. 2001). Recordings were obtained from the dorsolateral prefrontal cortex that included both the frontal eye fields and area 46 in all 4 monkeys. Two animals (JK and AZ) had additional recordings from areas 7a and 7ip in the posterior parietal cortex. Monkeys were implanted with a scleral eye coil to monitor eye position and a head bolt to stabilize the head during performance of the task (Judge et al. 1980). Surgery and training protocols were in accord with guidelines set by the National Institutes of Health, reviewed and approved by the Yale University Animal Care and Use Committee.

The animals were trained to perform an oculomotor delayed response (ODR) task. They initiated a trial by fixating a central point $0.1–0.2°$ in size, for 1 s, and continued to maintain fixation as a cue stimulus subtending $0.5–1°$ flashed for 500 ms at an eccentricity of $13–14°$. A delay period lasting 3 s followed the presentation of the cue, at the end of which the fixation point was extinguished and the monkeys were trained to make a saccade to the remembered target location. The cue could appear at one of 8 possible locations, equidistant around the fixation point and randomly interleaved from trial to trial. Ten to 12 correct trials were typically recorded for each location.

Neurophysiological recording

Neuronal activity was monitored using varnish-coated tungsten electrodes of $1–4$ MΩ impedance, at 1 kHz, as described in Chafee and Goldman-Rakic (1998) and Constantinidis et al. (2001). One or more electrodes were placed in stainless steel guide tubes and advanced into the cortex with the aid of a microdrive. Glass-coated Elgiloy metal microelectrodes ($0.6–1.5$ MΩ at 1 kHz) were used for a few experiments. Neuronal activity was amplified and band-pass filtered between 400 Hz and 10 kHz. For 2 animals (MAR and COD), the conditioned signal was sampled with a temporal resolution of 30 μs and waveforms were sorted into separate units using a template-matching algorithm (CED, Cambridge, UK). The data acquisition system was configured to classify voltage deflections into separate spikes if the peaks of the deflections were separated by about 1.5 ms, which is shorter than the absolute refractory period of most cortical neurons. Action potentials occurring at shorter intervals could not be correctly resolved. For the other 2 animals (JK and AZ) neurophysiological activity was sampled at 2-ms resolution and action potentials were classified into separate units using a waveform discriminator (Signal Processing Systems, 8701 waveform discriminator, Prospect,

South Australia). In practice, action potentials could not be stored as successive samples using this system, so the minimum separation of recorded action potentials was 4 ms.

Neurons were classified as regular spiking (RS) or fast-spiking (FS), putative pyramidal neurons and interneurons, respectively, based on their spike width and baseline firing rate, as described in detail elsewhere (Constantinidis and Goldman-Rakic 2002). Briefly, plotting the baseline firing rate against the width of spike waveform of each unit revealed 2 classes of neurons, one characterized by a longer spike duration and low firing rate and one characterized by shorter spike duration and high firing rate. Approximately 70% of the neurons located in the extreme of the 2 distributions were classified as FS or RS, respectively.

Neuron selection

Neurons analyzed in this study were selected from our database of recordings if they satisfied 2 criteria. They displayed activity that was significantly elevated during the delay period relative to the baseline and also exhibited spatial tuning; that is, this activity varied significantly for the 8 spatial locations tested with the ODR task (ANOVA test, $P < 0.05$). Some of the analytical techniques for evaluating the spectral properties of the spike train, described below, required a minimum total number of spikes. Given that 10–12 trials were collected per condition in most experiments, this essentially constituted a third requirement of firing rate greater than about 4 spikes/s. A total of 229 prefrontal cortical neurons from the 4 monkeys (169 from COD, 22 from MAR, 21 from JK, and 17 from AZ) that met these criteria were analyzed. For these neurons, we computed autocorrelograms, interspike interval (ISI) histograms, and power spectra for 3 conditions: *1*) the last 500 ms of the fixation period; *2*) delay period activity for preferred targets, that is, cue locations that elicited a firing rate above the average delay rate across all cues (solid circles in tuning curves of Fig. 4); and *3*) nonpreferred cue positions, those eliciting firing rates below the average delay rate (hollow circles in tuning curves of Fig. 4). Additionally, we also applied our analyses to 27 available multiunit recordings (from 2 monkeys) from which 2 or 3 units could be typically isolated.

Power spectrum analysis

In all cases power spectra were computed for each spike train considered, normalized by the expected power of a Poisson spike train at the same firing rate, and then averaged to reduce the variance. Averaging was thus always performed in the frequency domain and on normalized spectra. We computed the power spectrum of a neuronal spike train as described by Jarvis and Mitra (2001). These methods assume the stationarity of the point process analyzed. For this reason, we cut all the spike trains in overlapping 0.5-s windows and treated each window as a different trial of an independent stationary point process. Implicit is thus the assumption that nonstationarities in the data appear only at time scales longer than 0.5 s. A continuous process was built from the spike train by replacing each spike by a delta function and subtracting the average rate, and we subsequently processed these data with Fourier transforms to obtain the power spectra.

The raw estimate of the spectrum, that is, the magnitude-squared Fourier transform of the spike-train data is a biased and inconsistent (i.e., the variance does not decrease with increasing data length) estimate. Windowing the data with a suitable envelope function or *taper* reduces the bias. This taper function $h(t)$ is nonzero only within the time window of the data and is properly normalized: $\int_0^T h(t)^2 dt = 1$ (Percival and Walden 1993). To reduce the variance of the estimate (the windowed estimator is distributed as χ^2), one can either average over nearby frequencies (lag-window averaging) or use a set of envelope functions that are a complete set of basis functions for time- and frequency-limited functions. One such set of taper functions

constitutes the Slepian functions: a set of orthogonal basis functions that maximize the energy in a given time–frequency interval. Because the windows are an orthonormal set, the estimates of the spectra from each window are independent, and hence their average results in a low-variance estimate of the spectrum. We computed Fourier transforms on our spike trains windowed by the first 4 tapers of the Slepian sequences (Percival and Walden 1993). The power spectrum of the spike train estimated in this way was then normalized to the expected power of a Poisson spike train of the same mean rate and spectra from multiple behavioral trials were averaged together. The variance of the normalized spectra was calculated using a *jackknife method* (Thomson and Chave 1991). The jackknife variance is a powerful method of assessing the variance of samples without any assumptions about the underlying distributions, similar to the bootstrap. The resulting jackknife statistic is *t*-distributed. For Poisson data, the jackknife variance is a good approximation of the theoretical variance. Specifically, a series of spectrum ensembles were generated by leaving out one trial at a time and averaging over the remaining spectra. The jackknife variance was estimated as the variance across ensembles scaled by the number of degrees of freedom used to compute each member of the ensemble [tapers $\times (N_{\text{trials}} - 1)$]. The jackknife variance is a robust estimate, even in the presence of nonstationarities.

Coefficient of variation

From the series formed by the ISIs of each spike train we computed 2 measures of the ISI variability: the coefficient of variation (*CV*) and its local counterpart, CV_2. *CV* is obtained directly from the ISI histogram, by dividing its SD by its mean, $CV = \langle (\text{ISI} - \langle \text{ISI} \rangle)^2 \rangle^{1/2} / \langle \text{ISI} \rangle$. The *CV* measures how close the spike train is to an ideal Poisson spike train (for which $CV = 1$), assuming that the data are stationary. Because this assumption was violated by many of our data sets, we used a second measure of ISI variance, which we refer to as CV_2. CV_2 is computed by comparing each ISI (ISI_n) to the following ISI (ISI_{n+1}) to evaluate the degree of variability of ISIs in a local manner (Holt et al. 1996)

$$\langle CV_2 \rangle = \frac{1}{N-1} \sum_n CV_2(n), \quad CV_2(n) = \frac{2|\text{ISI}_{n+1} - \text{ISI}_n|}{\text{ISI}_{n+1} + \text{ISI}_n}$$

A Poisson spike train has $\langle CV_2 \rangle = 1$. For a Poisson spike train with absolute refractory period t_r, however, $\langle CV_2 \rangle$ is always smaller than 1. A straightforward calculation departing from the calculations in Holt et al. (1996) yields for a Poisson spike train of rate r and absolute refractory period t_r: $\langle CV_2 \rangle = 1 - rt_r \int_{rt_r}^{\infty} (e^{-x}/x)dx$, which is a nonmonotonic function of rt_r. This formula is used to compute t_r once $\langle CV_2 \rangle$ and r are known for a given spike train; these values then define the Poisson spike train with absolute refractory period t_r that best approximates the data. Furthermore, the probability density of the quantity $CV_2(n)$ for adjoining ISIs is given by

$$P(CV_2) = \frac{1}{2} e^{-rt_r 2/(2-CV_2)} + \frac{rt_r}{2} e^{-rt_r} \int_{rt_r CV_2/(2-CV_2)}^{\infty} \frac{e^{-x}}{x} dx$$

Thus for a Poisson spike train with absolute refractory period, CV_2 depends on the firing rate in a nontrivial fashion.

Bursting measures

To assess the degree of burstiness of a given collection of spike trains, we binned all ISIs and defined the following measures: fraction of ISIs <5 ms relative to the fraction of ISIs <5 ms in a Poisson spike train of the same mean firing rate (*B1*), fraction of ISIs smaller than the mean ISI divided by 10 (*B2*), or fraction of ISIs smaller than 5 ms (*B3*). Measures *B1* and *B2* applied to a Poisson spike train do not change as its rate is varied (in this sense, these measures are rate-independent). However, the measure of burstiness *B3* of a Poisson

spike train grows with its firing rate. All the results reported here for the autocorrelogram measure *A* (see following text) were paralleled by *B1* and *B2*. We therefore chose to report only the results for *A* for the sake of clarity.

Autocorrelograms

We calculated the autocorrelogram of a spike train as the histogram of the time intervals between any 2 spikes, from which the shuffle predictor was subtracted (the shuffle predictor was obtained as the average cross-correlogram of spike trains corresponding to different trials) and the result was normalized to the SD of the shuffle predictor at each time lag (see Aertsen et al. 1989). Thus the autocorrelogram is expressed in units of the shuffle predictor SDs. Our measure of burstiness/refractoriness in a spike train (*A*) is computed from the autocorrelogram: it is the average height of the central bins that correspond to a time lag <5 ms.

Cell type classification

We used 2 criteria to classify spike trains as "Poisson," "refractory," or "bursty": the departure of the power spectrum in the 5- to 60-Hz band relative to a Poisson spectrum of equal firing rate by more than one SD (bursty: excess power; refractory: suppressed power; Poisson: no structure more than one SD away), and the average height of the central autocorrelogram bins (*A*). We classified spike trains as bursty if their power spectrum exceeded the Poisson spectrum by more than one SD and *A* was >1 (central peak more than one SD above the shuffle predictor). Spike trains were classified as Poisson if their power spectrum did not deviate from their Poisson power spectrum by more than one SD and the value of *A* fell between −1 and 1. Finally, we classified spike trains as refractory if their power spectrum was suppressed relative to the Poisson spectrum by more than one SD and *A* was smaller than −1 (central trough more than one SD depressed with respect to the shuffle predictor). Notice that some power spectra could satisfy both the "bursty" and the "refractory" criteria and lead to a nondisjoint classification of spike trains. In those cases, we classify spike trains as "bursty" because spectral peaks are often accompanied by power suppression at adjoining frequencies. To classify one neuron according to its spiking characteristics as "Poisson," "refractory," or "bursty," we required that the corresponding classification criterion was satisfied for spike trains recorded in at least one of the 3 task conditions (fixation, delay after preferred targets, and delay after nonpreferred targets). Notice that this classification is nonexclusive: a given cell can belong to various classes. The use of the power spectrum shape to determine the burstiness of a spike train has been discussed by Bair et al. (1994).

Spectral classification techniques: Isomap

To compare spectra in an unbiased way we used the classification scheme Isomap, described by Tenenbaum et al. (2000). As in the case of multidimensional scaling (Mardia et al. 1979), the purpose of Isomap is to provide a visual representation of the pattern of proximities (i.e., similarities or distances) among a set of objects (here, power spectra). However, in contrast to multidimensional scaling (MDS), Isomap does not implicitly assume that distances are taken on a Euclidean manifold but allows for the more general case of geodesics on smooth non-Euclidean manifolds. Thus it is a powerful method to detect the underlying structure of the data without making a priori assumptions about its classifying aspects, and it succeeds in many more cases than classical MDS. In brief, pairwise distances between spectra are determined by using the Itakura–Saito distance

$$D = \log (\langle S_1(f)/S_2(f) \rangle) - \langle \log (S_1(f)/S_2(f)) \rangle$$

where $\langle \cdot \rangle$ denote the average over frequencies. The Itakura measure is a standard tool for calculating distances between spectra for automatic

speech processing. Only segments connecting each spectrum to its 4 closest neighboring spectra are then retained to construct a graph, along which *all* pairwise distances among spectra are recalculated. The table of distances along this graph is then fed into a classical MDS algorithm (Mardia et al. 1979) to find the best 2-dimensional embedding that preserves the geodesic distance. The output of Isomap consists of the coordinates of each spectrum in this 2-dimensional space. We will focus on the axis that accounts for most of the variance in the population of power spectra (in our graphs, the *x*-axis) and we will use this coordinate for each spectrum to compare its position in relation to other spectra and thus assess the significance of task dependencies in the shape of the power spectra.

Statistical tests

We used various statistical tests to assess the statistical significance of our results. When we used ANOVA tests, we first determined whether the data distributions, or their transformed values, deviated significantly from a Gaussian distribution (Jarque– Berra test, $P < 0.01$). We also tested the hypothesis of homogeneity of variances of our distributions through Bartlett's test, and we made sure that it could not be rejected at the significance level $P < 0.01$. Interaction effects of the factors considered in 2-way ANOVA tests were further analyzed by looking at the corrected means (Harwell 1998). When statistical tests showed that the data (or any transformation checked) was not compatible with a Gaussian hypothesis within our significance level, we used the nonparametric Kruskal– Wallis test (nonparametric version of one-way ANOVA) to assess significance, and we represented the data dispersion as median $\pm$ semi-interquartile range. Post hoc analyses were performed by means of a multiple comparison procedure.

All our data analysis was performed in the software package Matlab 6.

RESULTS

Discharge patterns

A wide range of discharge patterns was observed among the 229 neurons in our data base. Stereotyped patterns of discharge were classified as Poisson, refractory, and bursting as assessed through their autocorrelograms and their power spectra (see Table 1). The most frequent pattern in our database (Poisson discharge) had a virtually flat power spectrum, approaching that which would be expected for an ideal Poisson spike train. An example neuron is shown in Fig. 1*A*, exhibiting a flat autocorrelogram, an exponentially decaying ISI histogram, and a flat power spectrum. Approximately 89% of neurons (204/229) displayed (see METHODS for details on neuronal classification) a flat power spectrum ranging within one SD of the expected power of a Poisson spike train with the same firing rate. Sixty-eight percent of neurons (155/229) had a central peak in the autocorrelogram that did not differ by more than one SD (see METHODS) from their shuffle predictor ($-1 < A < 1$). In 63% of neurons (145/229), this stereotyped discharge pattern was present in both measures—the power spectrum and the autocorrelogram. This is the subpopulation of neurons classified as "Poisson" for our subsequent analyses.

Another pattern observed in the sample was characterized by autocorrelograms displaying a central dip and power spectra with significant troughs at low frequencies (Fig. 1*B*). A significant power spectrum trough in the band 5–60 Hz was identified in 38% of our neurons (87/229). Central dips in the autocorrelogram ($A < -1$) were clear in 39% of neurons

TABLE 1. *Classification of spike trains*

		Task Condition		
Measure	Classification	Fixation	Preferred	Nonpreferred
Spectrum	Poisson	81 (185)	49 (112)	76 (175)
	Trough	10 (22)	35 (81)	15 (35)
	Peak	10 (22)	16 (36)	8 (19)
Autocorrelogram (*A*)	Poisson	52 (119)	38 (87)	41 (94)
	Refractory	20 (45)	32 (73)	18 (42)
	Bursty	26 (59)	30 (69)	40 (92)
Spectrum + *A*	Poisson	48 (111)	24 (56)	35 (81)
	"Refractory"	6 (14)	24 (56)	10 (22)
	"Bursty"	8 (19)	12 (28)	8 (18)

Values are expressed as percentages; n = number of neurons (shown in parentheses). Classification of neuronal trains in the database according to two measures (Spectrum and *A*) and concurrently by both of them (Spectrum + *A*) for the three task conditions: fixation period, delay after preferred cues and delay after nonpreferred cues. The power spectrum identified neurons as belonging to one of the three classes depending on whether the power spectrum estimate in the frequency range 5–60 Hz is within one SD (Poisson), below (Trough) or above (Peak) by more than one SD, compared to the power expected for a Poisson spike train of the same firing rate. If a power spectrum showed a significant peak, it was counted in the "Peak" class, regardless of whether it also displayed a significant trough at a different frequency (see METHODS). The central bins of the autocorrelogram as indexed by *A* (see METHODS) classified neurons as Poisson for $-1 < A < 1$, as refractory for $A < -1$, or as bursty for $A > 1$.

(90/229). Neurons that could be characterized as "refractory" by both measures constituted 26% of all cells in our sample (60/229) and they constitute the class of "refractory" neurons in this study.

Bursting behavior was also present in our database. A cell displaying a representative bursting power spectrum is shown in Fig. 1*C*. The bursting behavior can be inferred by the sharp central spike of the autocorrelogram, the long tail of the ISI histogram, and by the power spectrum peak in the 20-Hz range. Bursting in this example did not depend on the epoch of the task, despite the marked differences in firing rates during the fixation period and the delay period, or on whether activity was recorded for the preferred or nonpreferred target. Out of 229 neurons 39 (17%) displayed power spectra with the power enhanced significantly over the expected value for a Poisson spike train in the band 5– 60 Hz. Autocorrelograms showed a marked central peak ($A > 1$) in 42% of the neurons (96/229). Overall, 14% of the cells in our sample (32/229, henceforth constituting the class of "bursty" neurons) displayed a "bursting" discharge pattern according to both the power spectrum and the autocorrelogram.

Task-dependent modulation of interspike intervals

We next tested whether the temporal patterns of prefrontal cortical neuron discharge varied systematically across different task conditions. Analysis of the coefficient of variation (either its global *CV* or local version $\langle CV_2 \rangle$; see METHODS) was higher during the delay than the fixation period but it was not very different between the delay conditions after preferred and nonpreferred cues (Fig. 2). This finding indicated that the coefficient of variation of the ISI was not a function of firing rate alone, as one would expect to observe a similar *CV* for fixation period and delay period after presentation of a nonpreferred target, which did not differ substantially in rate (13
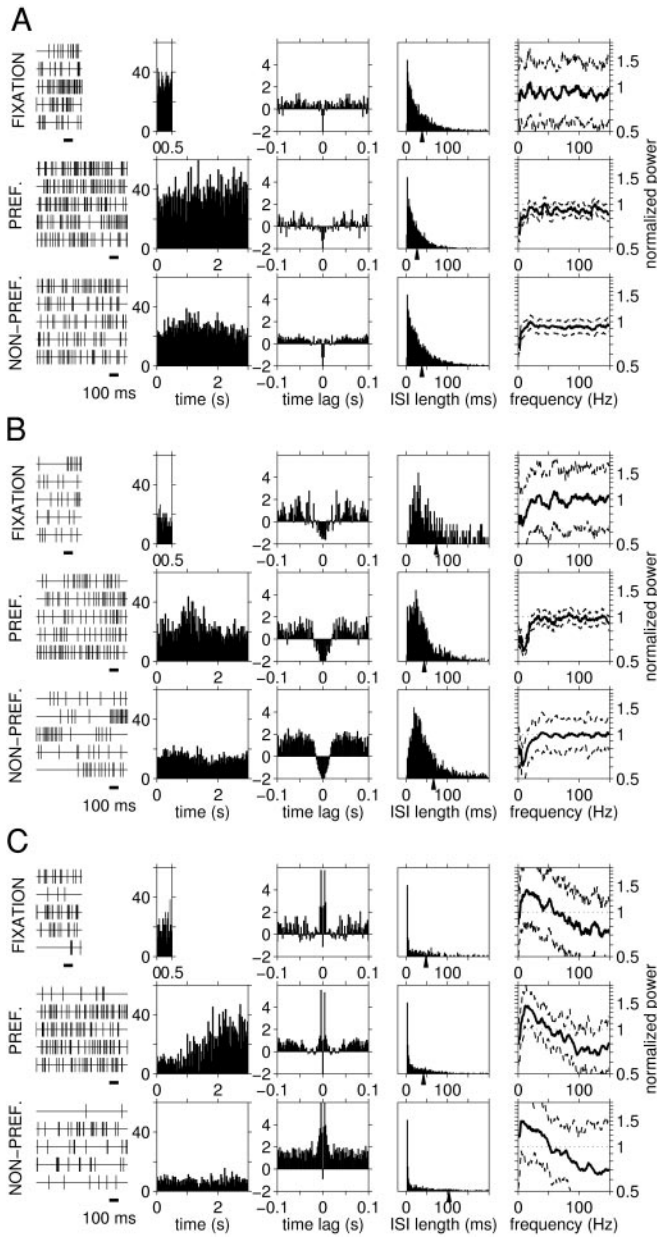
FIG. 1. Representative discharge patterns observed in database: Poisson (*A*), refractory (*B*), and bursting (*C*). All panels: *first row*: last 500 ms before cue onset (fixation epoch); *second row*: delay period after preferred cues; *third row*: delay period after presentation of nonpreferred cue. Columns depict, respectively, sample spike trains, poststimulus time histograms (*y*-axis in Hz), autocorrelograms, interspike interval histograms [arrowheads on *x*-axis indicate mean interspike interval (ISI)], and power spectra with associated error bars (dashed lines) positioned at one SD from mean (thick solid line). Vertical units of power spectra indicate power relative to expected power of Poisson spike train at same firing rate.

Hz in fixation and 11 Hz in delay/nonpreferred, average across all cells), and a significantly different *CV* for delays between preferred and nonpreferred targets, the rates of which were markedly different (18 Hz for delay/preferred and 11 Hz for delay/nonpreferred, average across all cells). This is confirmed in Fig. 2*A* (*bottom right panel*), where *CV* and $\langle CV_2 \rangle$ are shown not to depend on the mean ISI (correlation coefficient -0.03 for CV, and -0.2 for $\langle CV_2 \rangle$). The distribution of CV_2 for all adjoining ISIs across neurons belonging to each of the classes

(Poisson, refractory, and bursty in Fig. 2*B*, *bottom right panels*), shows that firing statistics of prefrontal neurons classified as "Poisson" are quite well described by a Poisson spike train with absolute refractory period, neurons in the "refractory" class have some systematic departures from this model but follow it qualitatively, and bursty neurons have a completely different CV_2 probability density, not captured by the model (as it should be expected). A second task-dependent effect was associated with the degree of bursting in the spike trains (Fig. 3). Based on the central peak in the autocorrelogram (*A*), spike
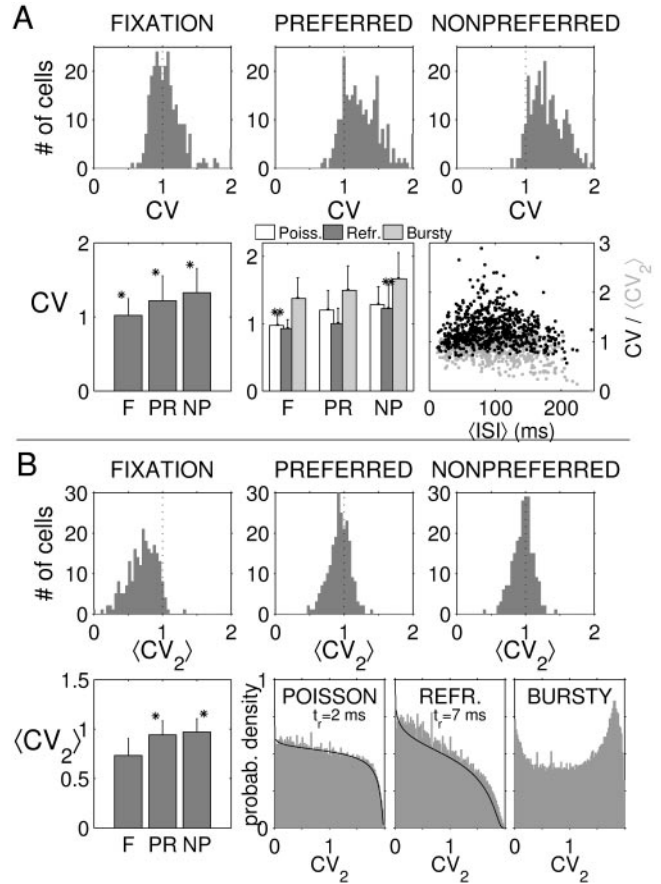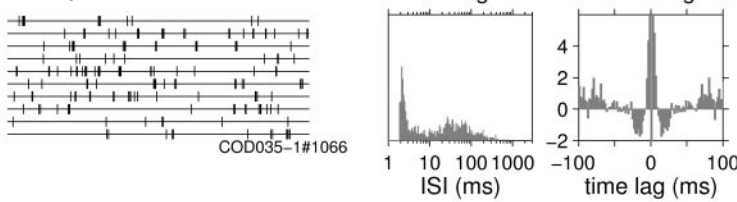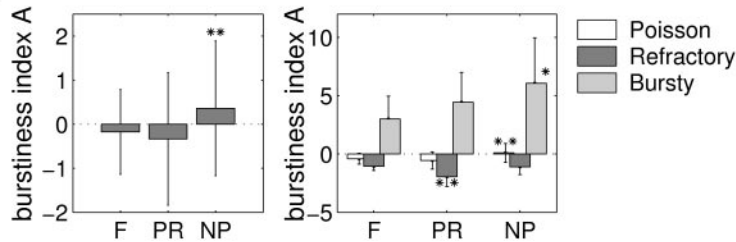

FIG. 2. Task-dependency in variability of neuronal responses. Both global (*CV*, in *A*) and local ($\langle CV_2 \rangle$, in *B*) measures of ISI variability increase significantly during delay period compared with fixation epoch. All panels: *Top row*: histograms for *CV* or $\langle CV_2 \rangle$ (data from all neurons in database) for each task condition. *Bottom row*: graphs on *left* show mean and SD in each task condition (F, fixation; PR, delay after preferred cue; NP, delay after nonpreferred cue). This is also shown separately in case of *CV* (not shown for $\langle CV_2 \rangle$ to avoid redundancy) for 3 classes of neurons identified using both burstiness measure *A* and power spectrum (*middle graph* in *A*). *Bottom right graph*, *A*: *CV* (and $\langle CV_2 \rangle$, in gray) vs. mean ISI is plotted for all neurons and task conditions in database. *Bottom right graphs*, *B*: probability density of CV_2 as estimated from empirical data (gray histograms, data from adjoining ISIs in cells and trials combined, for each population of cells identified using both spectrum and *A*) or as expected for Poisson spike train with absolute refractory period of same mean rate and same $\langle CV_2 \rangle$ (black solid line, computed using formulae in METHODS. Resulting refractory times t_r are indicated. Stars indicate that significance level for rejection of null hypothesis was reached and location of star with respect to corresponding error bar indicates for what adjoining task condition difference of means reached significance. Significance was determined using 2-way unbalanced ANOVA ($P < 0.01$) and multiple comparison procedure on data transformed according to log ($CV - 0.5$) in *A* and $\langle CV_2 \rangle$ 2 in *B*, and for factors task and monkey in *left histograms* and task and cell type in *right histograms* in *A*. No significant interaction found for task and monkey nor between cell type and task.

FIG. 3. Task dependency in occurrence of bursts. Our measure of burstiness (*A*) shows that burstiness is enhanced significantly during delay if cue was presented at nonpreferred location. *Top panels*: example for bursty neuron (sample spike trains, ISI histogram with logarithmic *x*-axis and autocorrelogram). In all other graphs, thick bars show median across all cells or indicated subpopulation of cells (Poisson, refractory, or bursty; see classification details in METHODS), and error bars indicate magnitude of semi-interquartile range; star indicates that null assumption of equal medians could be rejected (see METHODS for meaning of stars' locations) at significance level $P < 0.01$ using multiple comparison procedure after Kruskal–Wallis test. F, fixation; PR, delay after preferred cue; NP, delay after nonpreferred cue.

trains in the delay period after a *nonpreferred* target were typically more bursty than either the fixation or the delay period after a preferred target. This also held for neurons classified as Poisson or bursty. However, for cells in the "refractory" class the magnitude of the zero-lag dip increased significantly in the delay period after a preferred cue compared with the other 2 conditions (similar results were obtained from burstiness measures derived from the ISI histogram, not shown). These results indicate that some temporal patterns of spike trains (e.g., burstiness) are independent of firing-rate modulation.

Task-dependent modulations of power spectra

To explore more systematically the modulations in temporal structure of spike trains, we focused on their power spectra.

Power spectra can be normalized and error bars can be computed for each point, thus making them a convenient analytical tool for comparisons across task epochs and for determining significant differences. From visual inspection, marked changes in power spectra were not evident in the various epochs of the task. However, weak task modulations were apparent in many cases. Figure 4 shows 3 examples of task-dependent modulations in the power spectrum shape observed in individual neurons of our database. The most frequent task dependency (36/229 neurons, 16%) was a marked deepening of a low-frequency trough in the delay after a preferred cue (Fig. 4*A*). This was the most salient task-dependent effect observed when we averaged power spectra across the population of neurons (Fig. 5). The effect was consistent across all monkeys and was observed both in the dorsolateral prefrontal cortex, as
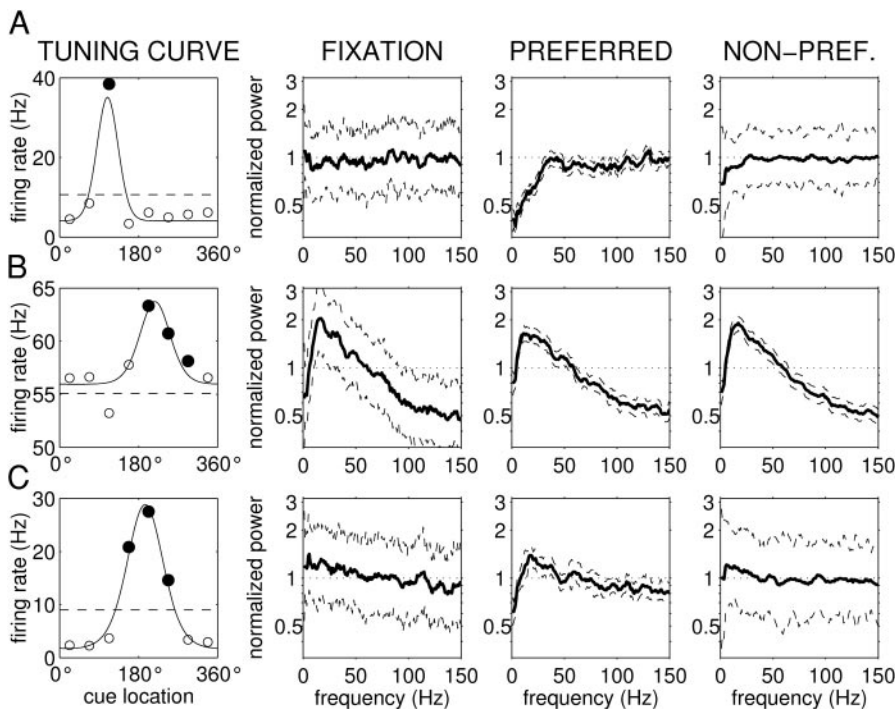

FIG. 4. Sample task-dependent changes in power spectra of single neurons. Most frequent task-dependency was suppression of power at low frequencies during delay epoch after presentation of preferred cue (*A*, found in 36 of 229 neurons). Other task-dependencies observed more rarely involved suppression (*B*, 6/229) or enhancement (*C*, 6/229) of peaks during delay period after preferred cue. *First panels*, *left*: tuning curves for each cell shown here. *Second panels*, *left*: spectra computed from spike trains recorded during fixation. *Third panels*: power spectra from delay period after preferred cue presentation (i.e., all cues that elicited higher average firing rate than average across all 8 cues and all trials, solid circles on tuning curve) and *rightmost panels* are obtained from delay period data, when presented cue was none of the cues preferred by cell (hollow circles on tuning curve). In power spectra, solid lines follow mean spectra across trials and dashed lines are error bars obtained by mean ± 1 SD. All spectra are in log units on *y*-axis and are normalized to power expected for Poisson firing.
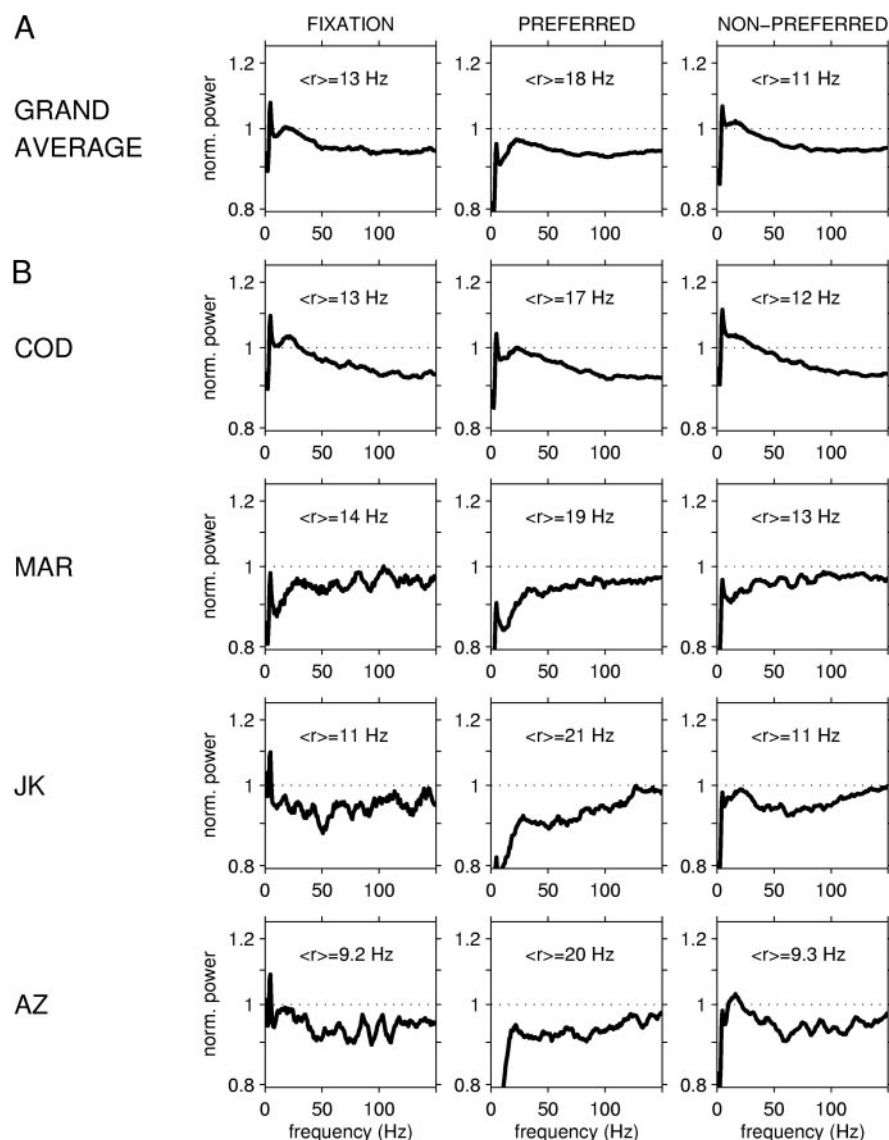
FIG. 5. Major task dependency observed by averaging together power spectra from different cells is power suppression at low frequencies in spike trains recorded during delay epoch of task after presentation of preferred stimulus. *A*: spectra averaged across all 229 neurons in database for each task condition (fixation, delay-preferred, delay-nonpreferred). *B*: spectra averaged across all cells on monkey by monkey basis. Average firing rates ($\langle r \rangle$) across populations are indicated in each panel. Because of difference in neuron number recorded from each monkey, grand average is dominated by power spectra from COD.

shown here, and in the posterior parietal cortex (monkeys JK and AZ, data not shown).

In contrast, only a few cells showed power spectra with clear peaks. The neuron in Fig. 4*B* had a clear peak in the power spectrum that was slightly decreased during the delay period after a preferred target (dependency shared by 6/229 neurons, 3%). Another task-dependency observed (6/229 neurons, 3%) was an enhancement of a peak in the spectrum during the delay, after the preferred target (Fig. 4*C*).

An averaged spectrogram of 229 neurons was computed for trials in which the cue elicited a delay firing rate above average (preferred cue condition, Fig. 6*A*) and also for nonpreferred cues (Fig. 6*B*). We observed very little difference between the spectral properties of neuronal firing before and after cue presentation except for a suppression of power at low frequencies (<20 Hz) after the presentation of preferred cues (Fig. 6*A*). The spectrogram shows the time course of this suppression of power: it began during cue presentation and persisted throughout the delay period. For trials with nonpreferred cues only a slight power increase at low frequencies was observed (<20 Hz; see Fig. 6*B*).

Classifying power spectra shapes

To make a more unbiased comparison of the spectra across task epochs, we used the classification scheme Isomap (Tenenbaum et al. 2000). The classification obtained this way is unbiased in the sense that the major differences between the spectra are decided by the algorithm rather than a predetermined spectral feature that we are interested in (for details see METHODS). The resulting 2-dimensional map is shown in Fig. 7. Note that the principal axis, which accounts for most of the variance (*x*-axis), separates spectra that show a peak (large positive values of *x*) from those that show a pronounced trough (large negative values of *x*). This is shown more clearly in Fig. 8*A*, where the position of a spectrum on the *x*-axis of the Isomap was found to correlate remarkably well with the average power in the 5- to 20-Hz band, whereas it correlated only weakly with the average power in the band 20–60 Hz. Even this weak correlation with the 20- to 60-Hz power range can be accounted for by the correlation of the latter with the power in the 5- to 20-Hz band (Fig. 8*A*, *right panel*). This result confirms our previous observation that the most significant struc-

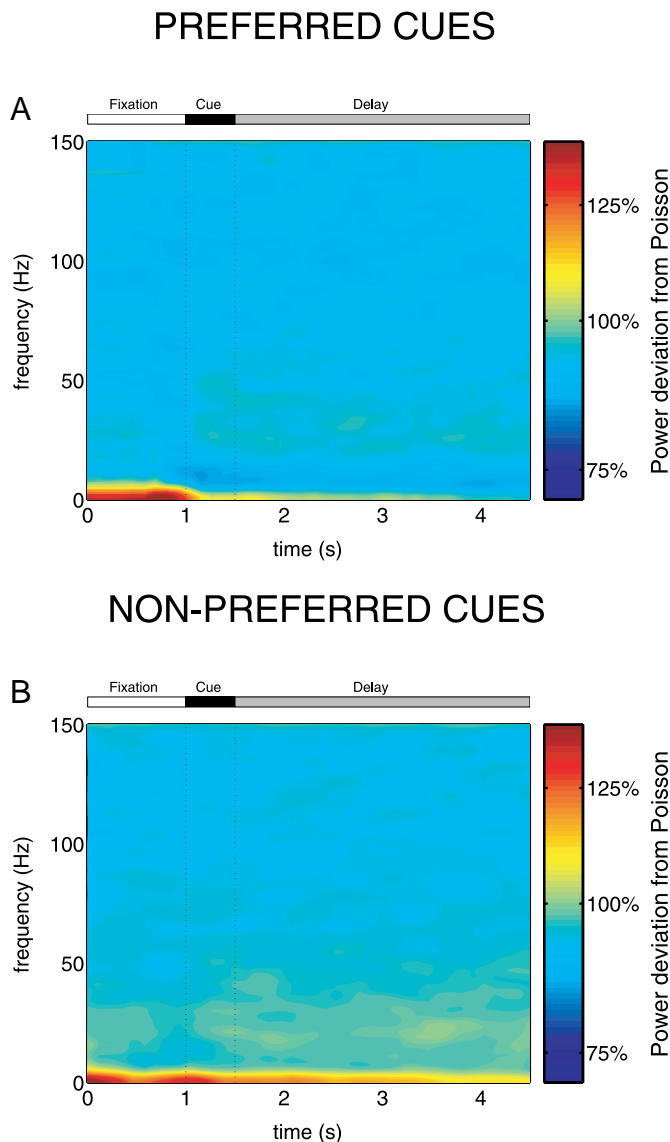## PREFERRED CUES

A

NON-PREFERRED CUES

B

FIG. 6. Power suppression at low frequencies after presentation of preferred cues starts at cue onset and is maintained throughout delay period as shown through spectrogram averaged over all neurons in database (*A*). For nonpreferred cue presentation (*B*) spectrogram does not vary systematically for neurons of our database during course of task. Power spectra features at very low frequencies (<5 Hz approx.) are not reliable because of finite length of our spike trains. Spectrograms were computed by averaging normalized power spectra calculated over 500-ms-long windows overlapped 250 ms from recorded spike trains.

tures in the power spectra occur at low frequencies (<20 Hz) and it is in that frequency range that the spectra distinguish themselves from one another.

We proceeded to test whether there was any correlation between the principal coordinate of each spectrum on the Isomap and the degree of bursting of the corresponding spike trains. Bair and colleagues (1994) reported that bursty cells typically show a peak in the power spectrum. If peaks in the spectra of our database are primarily caused by bursty firing rather than by nonbursty periodic firing we would expect to see a pronounced correlation between the principal coordinate of the spectra and the bursting of the spike trains. This was indeed so, as shown in Fig. 8*B* (*right panel*).
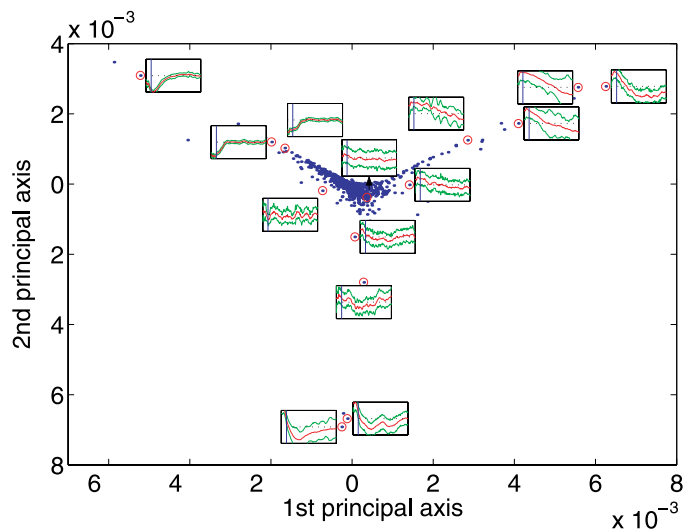

FIG. 7. Unbiased, 2-dimensional classification of all power spectra in database (*Isomap,* see METHODS) neatly separates peaks (positive *x*-coordinate) from troughs (negative *x*-coordinate) and clusters majority of spectra on central region corresponding to Poisson-like power spectra. As explained in METHODS, algorithm *Isomap* represents each power spectrum as one point in a multidimensional functional space, and computes 2-dimensional projection map that best preserves geodesic distances between spectra (shown by blue dots, one dot per spectrum). Some power spectra are explicitly plotted on map next to their location (highlighted with red circle) to show how output of *Isomap* responds quite accurately to our intuition of separating spectra showing peaks and troughs. Units of map axes are arbitrary and their values are used only to compare spectra locations to each other.

We also investigated how the electrophysiologically identified classes of RS and FS neurons related to the classifications of the spike trains that we have used here: Poisson, refractory, and bursty neurons. This classification showed a significant
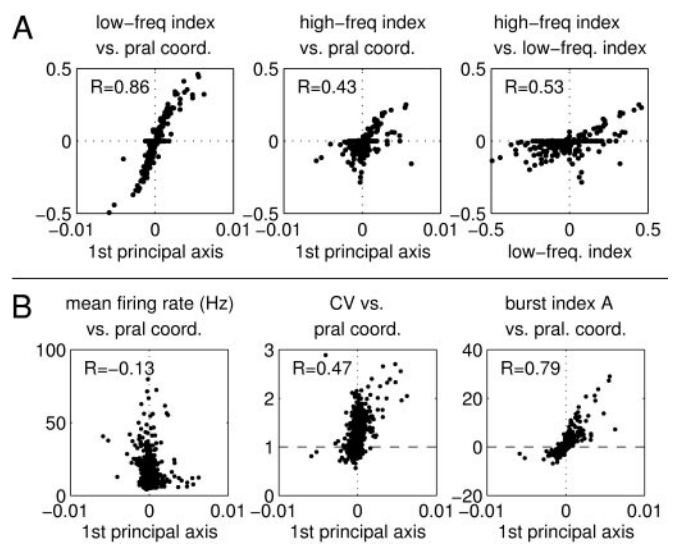

FIG. 8. Locations (*x*-coordinate or principal coordinate) of spectra on map of Fig. 7 correlate well with average power in band 5–20 Hz (*A, left panel,* low-frequency index) but not with average power in band 20–60 Hz (*A, middle panel,* high-frequency index) because all correlations observed there can be accounted for by correlation between high-frequency index and low frequency index (*A, right panel*). Principal coordinates of spectra also correlate poorly with firing rate of associated spike trains (*B, left panel*). In contrast, coefficient of variation (*CV*) and especially burstiness measure *A* strongly correlate with Isomap principal coordinate (*B, middle* and *right panels*). Correlation coefficients (*R*) are indicated in each panel.
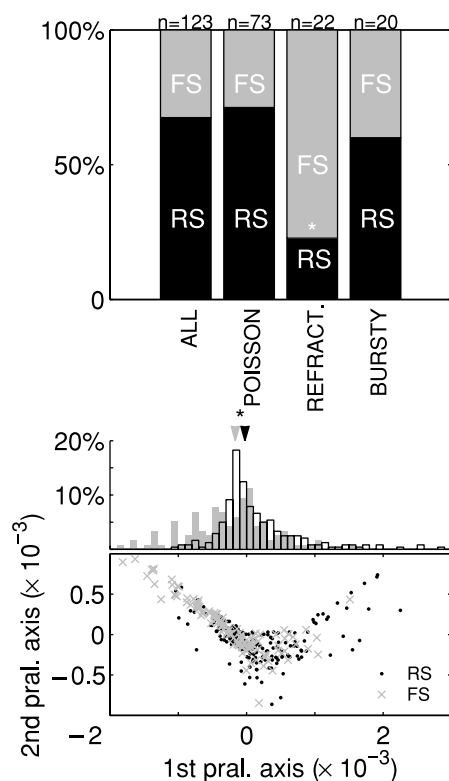
FIG. 9. Abundance of electrophysiologically identified fast-spiking neurons (FS) relative to regular spiking (RS) neurons was significantly larger among those cells classified as "refractory" by any of our criteria (see METHODS). *Top panel*: proportion of FS putative interneurons and RS putative pyramidal neurons, as classified based on their action potential and firing rate characteristics, in all electrophysiologically identified neurons (*first bar*), and in each classification of their spike trains according to both our spectral and burstiness measures (Poisson, refractory, bursty). When either classification criterion (burstiness and spectral shape; see METHODS) was used alone, similar results were obtained. *Bottom panel*: location on map of Fig. 7 of RS (black dots) and FS (gray crosses) neurons and histogram of their *x*-coordinate (RS, black hollow histogram; FS, gray solid histogram), showing slight but significant shift of FS neurons' locations toward *left* of map. Statistical significance in *top panel* was assessed by using χ^2 to analyze corresponding contingency table. The Null hypothesis that the probability of recording a RS or FS neuron is independent of burstiness and spectral properties (in 5–60 Hz range) of their spike trains was rejected at significance level of $P < 0.02$. In *bottom panel*, we used nonparametric Wilcoxon rank sum test to reject the hypothesis of equality of means for locations of FS and RS neurons in the map of Fig. 7 ($P < 0.01$).

effect, in that FS neurons are overrepresented among refractory neurons (Fig. 9). This result is similar to the observation from behaving rats that FS putative interneurons tend to be characterized by autocorrelations with a large dip at zero time lag (Csicsvari et al. 1999). Also, an overrepresentation of RS neurons was observed among neurons with *very high* bursting (for A >5 there are 18 neurons classified as RS and 1 as FS, the same effect is seen in the power spectra; see histogram tails in Fig. 9), in agreement with previous results (Constantinidis and Goldman-Rakic 2002).

We then examined whether the shape of power spectra, as classified by the Isomap algorithm, varied depending on the task conditions (Fig. 10). To assess that, we considered for each cell the Isomap location of its spectra corresponding to fixation, delay after preferred targets, and delay after nonpreferred targets (two examples in Fig. 10, *left top panels*). For each set of 3 power spectra associated with a given neuron, we calculated their center of mass along the principal axis (crosses

in Fig. 10) and recorded the signed distance "*r*" between the location of each of the spectra and their center of mass, along the Isomap principal axis. A positive value of *r* indicates that a spectrum corresponding to a particular task condition was shifted toward the "peak"-side of the Isomap with respect to the other task conditions. The 2 examples shown in Fig. 10 indicate the *r* value associated with the spectra shown in Fig. 4. The 2 spectra displayed opposite sign *r* values, as the Isomap classification distinguishes peaks and troughs. When the *r* values for spectra in each of the behavioral conditions were computed, the resulting empirical distributions were tested against the hypothesis of the equality of means (Fig. 10). There was a clear tendency, consistent across monkeys, of power increase at low frequencies (positive *r*) in the delay period after nonpreferred targets, whereas trough deepening (negative *r*) was typical in the delay period after preferred targets. Spectra for spike trains recorded during fixation were typically close to the center of mass of the 3 conditions.

Finally, we analyzed a smaller sample of multiunit recordings along the main lines of our single unit analysis. The results are illustrated in Fig. 11. Because of the small sample, some effects observed in single units did not reach significance (task dependency of burstiness, Fig. 11*B*; and task dependency of spectral shape, Fig. 11*C right panel*). Other results, however, were indeed replicated: variability of the ISIs (*CV* and $\langle CV_2 \rangle$) also increased significantly in the delay (Fig. 11*A*), and the main feature of the power spectra was their structure at frequencies below 20 Hz (Fig. 11*C*, *left panel*. As for single units in Fig. 8*A*, the high-frequency index did not correlate more with the principal coordinate than with the low-frequency index, not shown), which correlated very well with the degree of burstiness of the spike trains (Fig. 11*C*, *middle panel*). No overall increase of spectral peaks or troughs relative to single-unit recordings was revealed in the multiunit records.

DISCUSSION

We performed an analysis of the temporal structure of prefrontal neuron spike trains during the fixation and delay periods of a working memory task. Our main findings are threefold. First, the variability of ISIs for a neuron is typically higher during the mnemonic delay period than during the fixation period, regardless of whether the cue is preferred or nonpreferred. Second, the spectral properties of neuronal discharges in most neurons approximated the characteristics of a Poisson process. In a minority of cells that deviated significantly from the expected Poisson pattern, some showed a trough at low frequencies of the power spectrum and a pronounced dip near zero time lag of the autocorrelation function; others displayed a peak (at <20 Hz) in the power spectrum associated with the burstiness of spike discharges. Third, we observed a small but significant task dependency in the spike-train temporal structure. Neuronal firing during the delay period for preferred locations was characterized not only by elevated firing rate, but also by spectral power of low (<20 Hz) frequencies suppressed below the expected power spectrum of Poisson spike train. This power suppression was most prominent in FS neurons (putative interneurons).
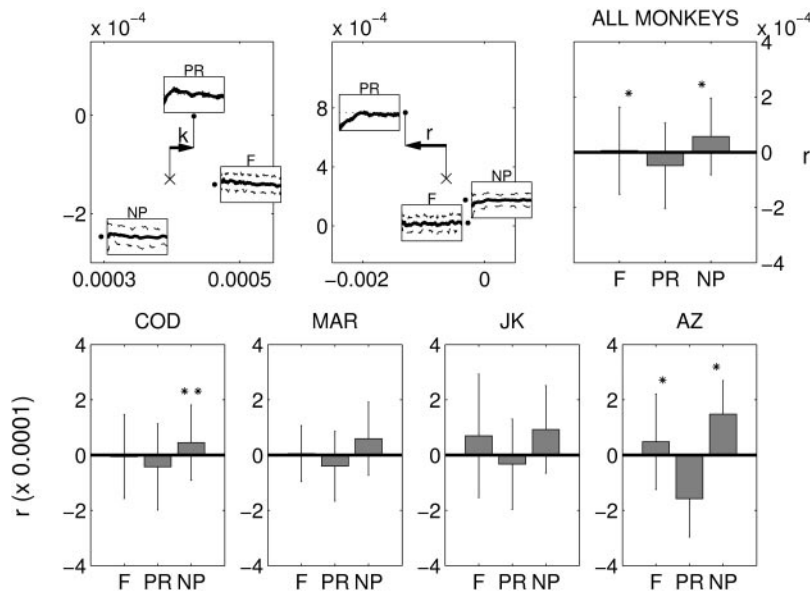
FIG. 10. Task dependency in location of spectra on Isomap of Fig. 7 reveals significant effects. For all monkeys, delay period after preferred cue was characterized by low-frequency (<20 Hz) power suppression (or shift to *left* along principal coordinate axis) and delay after nonpreferred showed typically shift to *right* along principal coordinate axis (consistent with bursting effect observed in Fig. 3). Task dependency was assessed by means of quantity *r*. As illustrated in examples of *top left panels* (same neurons as in Fig. 4), *r* is distance along principal axis of each spectrum to center of mass (crosses) of 3 spectra obtained for that given neuron in various task conditions (F, PR, NP). *Bar plots* [for all monkeys together and for each one of them (COD, MAR, JK, AZ)]: mean value of *r* for each task condition (gray bars) and its SD (error bars). Null assumption of equal means across data were tested by means of 2-way unbalanced ANOVA and multiple comparison procedure within significance level $P < 0.01$. No interaction effect was observed between task and monkey and hypothesis of equal means across monkeys could not be rejected. There was, however, a consistent effect in task showing that *r* is typically larger for delay after nonpreferred cues than otherwise. F, fixation; PR, delay-preferred; NP, delay-nonpreferred.

General characteristics of spike train temporal properties

We identified 2 types of deviations from the expected power spectrum of a spike train with Poisson characteristics: spectral peaks and troughs. Both of these were almost always observed in frequencies below 20 Hz. Significant spectral peaks were strongly correlated with increased burst firing. Previous studies have shown that firing of action potentials in bursts produces power spectral peaks, even when bursts themselves are not repeated periodically, with a constant interburst interval (Bair et al. 1994). Our current results are in agreement with these findings. Burst discharges are characteristic of a subclass of pyramidal neurons in the cortex (Connors and Gutnick 1990; Gray and McCormick 1996). Recent work suggests that bursts may subserve special types of coding and computations in sensory neurons (Doiron et al. 2003; Kepecs et al. 2002). What may be the significance of burst firing to the working memory circuits in the cortex? One possibility stems from the evidence that excitatory synapses in the prefrontal cortex exhibit short-term facilitation (Hempel et al. 2000). Hence bursts may represent a reliable neural signal through unreliable yet facilitating synapses (Lisman 1997; Wang 1999a), thereby contributing to the synaptic reverberation in the prefrontal circuits.

Our data show that a great proportion of neurons showing a significant dip in the autocorrelation function and power suppression at low frequencies are classified from the shape of the recorded spikes as FS neurons (putative interneurons). This is consistent with a physiological study of behaving rats reporting that FS interneurons tend to show a pronounced dip at zero time lag of their autocorrelations (Csicsvari et al. 1999). Such a dip in the autocorrelation and power suppression at low frequencies are usually related to an effective refractoriness in the neuronal spike train. Therefore interneurons apparently engage more importantly in this task-induced enhancement of the refractoriness of their output. The cellular and synaptic
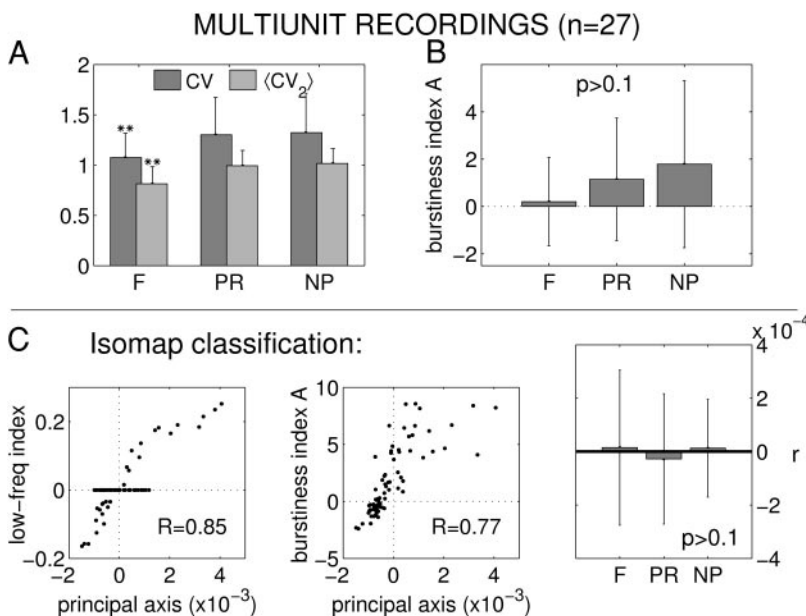

FIG. 11. Smaller sample of multiunit recordings ($n = 27$) reveals similar results to single units when statistical significance is reached. *A*: both *CV* and $\langle CV_2 \rangle$ increase significantly (ANOVA $P < 0.02$) during delay period, irrespective of whether target elicited high (PR) or low (NP) firing rate. *B*: burstiness of multiunit activity showed tendency to significant result obtained for single units (enhanced burstiness for delay after nonpreferred cue), but did not reach significance. *C*: Isomap classification also showed very good correlation with power at low frequencies (5–20 Hz, *left panel*) and with burstiness of spike trains (*middle panel*). However, weak task dependency of principal coordinate observed for single units (see Fig. 10 for details) did not reach significance for multiunit activity.

mechanisms, and functional implications, of this effect are currently unknown. Inhibition has been identified by computational models (Brunel and Wang 2001; Camperi and Wang 1998; Compte et al. 2000; Tegnér et al. 2002) as well as neurophysiological studies (Funahashi et al. 1989) as a mechanism responsible for the suppression of firing with respect to baseline for those pyramidal neurons nonselective to the cue during the delay. The contribution of temporal dynamics of interneuronal spike discharges to the generation of such suppressive inhibition is an important issue to be elucidated in the future.

Absence of oscillatory discharges in the autocorrelation and power spectrum

Since the original descriptions of oscillatory firing in the primary visual cortex of the anesthetized cat (Eckhorn et al. 1988; Gray et al. 1989), there have been several studies in the cat and monkey that failed to detect oscillatory firing, or reported that such oscillations were largely unrelated to the properties of visual stimuli (Bair et al. 1994; Ghose and Freeman 1992; Tovee and Rolls 1992; Young et al. 1992). Other investigators detected oscillatory firing but in a smaller proportion of the neurons tested (Bringuier et al. 1997; Cardoso de Oliveira et al. 1997; Nowak et al. 1995; Schwarz and Bolz 1991). Our present results add to this debate because truly oscillatory discharges were very rare in the spike trains of prefrontal cortical neurons. Some obvious factors that could be responsible for discrepancy among the various studies, such as the use of anesthesia, stimulus-induced periodicities, analysis criteria, and species differences, have been addressed by subsequent studies (Eckhorn et al. 1993; Friedman-Hill et al. 2000; Frien et al. 1994; Fries et al. 2001; Gray and Viana Di Prisco 1997).

The present study was designed to test the central hypothesis that elevated firing rate during the delay period following a target in the neuron's memory field was associated with oscillatory discharges, as suggested by Lisman and Idiart (1995) and Tallon-Baudry et al. (2001). Our present results suggest that, at least in individual neurons of the prefrontal cortex, this is clearly not the case. Power enhancement over the expected value for a Poisson spike train occurred only at frequencies below 20 Hz, and they were not related systematically to the behavioral task in any of 4 monkeys. This is in contrast to similar analysis performed on single-neuron recordings and local field potentials in posterior parietal cortex (Pesaran et al. 2002). Pesaran and colleagues detected significant task-related power increase in the gamma band in single parietal neurons. The spectral techniques employed there are analogous to the ones that we apply here. The only differences in the technical aspect of the analysis are their inclusion of non-memory-selective (according to the firing rate) neurons, the database size (40 neurons in their study vs. 229 neurons in the present study), and our unbiased classification through the Isomap method. It seems unlikely that these reasons can entirely account for such contrasting results. This raises the possibility that neurons in the prefrontal cortex have less propensity to display oscillations than those in the parietal cortex. A number of computational studies have shown that oscillations are detrimental to working memory function sustained by local cortical reverberation (Compte et al. 2000; Tegnér et al. 2002;

Wang 1999b). For example, suppression of oscillatory activity results in a greater tolerance to intervening stimuli (Compte et al. 2000). There is evidence that working memory-related activity in the prefrontal cortex is more resistant to distracting stimuli than in other cortices, like the inferotemporal cortex and posterior parietal cortex (Constantinidis and Steinmetz 1996; Miller et al. 1996; Sakai et al. 2002). Thus the absence of oscillatory activity in prefrontal single units during a delayed response task could reflect the stability of persistent activity supported by local cortical reverberation, and, at the same time, resistant to distracting stimuli.

Studies with recordings from motor cortex reported maximal rhythmic firing during periods preceding the onset of a cue and reduction of spectral power after the instruction for a particular movement, even though the firing rate modulation of single neurons follows the opposite pattern (Baker et al. 2001; Murthy and Fetz 1996; Sanes and Donoghue 1993). These results led to the suggestion that oscillatory firing in the motor cortex may be associated with a higher level of attention or arousal, in anticipation of a sensory event, rather than with the encoding of stimulus information per se. However, we do not find oscillatory firing in prefrontal neurons recorded during the oculomotor delayed response task, even though this task requires substantial attention allocation throughout each trial. Furthermore, the power suppression detected during delay for preferred cues cannot possibly be associated with a release of attention because that is the period of the task most demanding in terms of attentiveness for the animal.

The possibility remains that oscillations at the population level are not easily detectable at the level of firing patterns of individual neurons (Brunel 2000; Brunel and Wang 2003; Csicsvari et al. 1999). Indeed, the data we analyzed here correspond to single-neuron activities. Moreover, we noted that the results held for a smaller sample of multiunit recordings incorporating 2 or 3 units each (Fig. 11). On the other hand, the identification of task-related oscillatory activity has found its strongest evidence in measures of global activity of a large ensemble of neurons, such as local field potential (Pesaran et al. 2001) or intracranial EEG recordings in the occipital and parietal lobes (Raghavachari et al. 2001; Tallon-Baudry et al. 2001) during delayed response tasks. Oscillations may be more readily apparent in multiunit recordings, given that such recordings increase the probability that one of the units will display oscillations, and even more so in local field potentials. Unit isolation therefore may be partly responsible for the large differences in percentage of neurons displaying oscillatory firing in different studies. Therefore it would be interesting to undertake local field potential recordings from the prefrontal cortex during activation of working memory. The functional significance of rhythmic firing, detectable only in the activity of large numbers of neurons, as exemplified by local field potentials, but not in the spiking output of individual neurons, remains unclear at the present time.

Power spectral changes related to memory function

Neurons in our database showed little change in the spectral characteristics of their spike trains between the fixation and the delay periods, irrespective of whether the cue was preferred or nonpreferred. Assuming that the spectral features of a spike train are primarily affected by the degree of attentiveness

required for a task, the fact that there were no major differences in modulation of power spectra between the fixation and delay periods in the present database could be explained on the basis that the fixation requirement in an ODR task also requires substantial sustained attention.

Nevertheless, small but significant spectral effects of the task could be detected. We used the Isomap method to quantify the power spectrum's structure. We found that the first principal coordinate of the Isomap correlates well with the average power in the 5- to 20-Hz band, and distinguishes the presence of a trough or peak in that frequency range. Using this measure, and consistently for all 4 monkeys, we found that the spectral signature of active memory maintenance in single prefrontal neurons is a suppression of power at low frequencies (<20 Hz) if the cue presented is preferred, and a slight enhancement of power if the cue is nonpreferred (Fig. 10). A similar phenomenon has been observed in posterior parietal cortex during this same task (Fig. 5 in Pesaran et al. 2002), although there a power increase in the gamma band was also very prominent. It is thus possible that refractoriness is a shared signature for single neurons during working memory across cortical areas, whereas gamma band oscillations are a result of the local network connectivity and much more robust in parietal cortex than in prefrontal cortex. The comparison of our results with those of Pesaran et al. (2002) leads to the hypothesis that, in spike trains recorded during working memory, task-dependent power suppression below 20 Hz and gamma-band power increases are attributed to distinct mechanisms. As discussed in the following text, we also provide suggestive evidence that interneurons might be involved in the generation of the power suppression effect below 20 Hz.

Temporally irregular nature of persistent neural activity

We found that the ISI's coefficient of variation (CV) of a prefrontal neuron is consistently high (see also Shinomoto et al. 1999). Previous studies have reported that the ISI CV of visual cortical neurons in response to a fixed sensory stimulus is close to 1, the value for a Poisson process (Sofkty and Koch 1993). When the stimulus is naturalistic and time-varying (videos), the CV of V1 and inferotemporal neurons is as high as 1.8–1.9 (Baddeley et al. 1997). In the latter case, the large CV may be directly related to the slow temporal changes of the neural firing rates. Here we report that during the delay period of an oculomotor task, when there is no external stimulus and the monkey's eye position is maintained, the CV of mnemonic activity of prefrontal neurons is above 1, on average, and larger than during the fixation period, regardless of whether the cue is preferred or nonpreferred. Single-neuron modeling shows that, generally, the CV is larger when the neuron fires at a lower rate (Liu and Wang 2000; Sofkty and Koch 1993; Troyer and Miller 1997) or is more bursty (Wilbur and Rinzel 1983). Therefore when the cue is nonpreferred, a larger CV of the delay activity may be explained by a lower firing rate (compared with the fixation period) and perhaps by a slightly higher propensity of burstiness across the neural population (as observed in Fig. 3). On the other hand, when the cue is preferred, the neuronal firing rate is higher (up to more than 60 Hz), and burstiness is smaller, yet the CV is still larger. Whether this high CV of prefrontal neurons is a result of slow temporal changes of delay period activity (see, for example, Chafee and

Goldman-Rakic 1998; Romo et al. 1999) or reflects the balanced dynamics between synaptic excitation and inhibition (Shadlen and Newsome 1993) in the working memory circuit, remains to be explored in the future. Also, the incidence of task-dependent burstiness could be significant because it has been shown that fluctuations of neural activity and synaptic inputs at low or high frequencies may have differential impacts on the reverberatory network dynamics (Nowak et al. 1997).

The observed irregularity of persistent activity has potentially important implications. Because high variability of neural discharges is likely to originate from stochastic synaptic bombardments (Shadlen and Newsome 1993; Shu et al. 2003; van Vreeswijk and Sompolinsky 1996), our result is consistent with a network mechanism for generating mnemonic delay activity in the prefrontal cortex. By contrast, it is unclear how the high ISI variability could be explained if persistent activity is a single-neuron phenomenon (Egorov et al. 2002). Moreover, the scenario of balanced synaptic excitation and inhibition (Shadlen and Newsome 1993; van Vreeswijk and Sompolinsky 1996), proposed to account for a high CV close to 1, does not seem to be compatible with the premise of multistability between a resting state and active memory states (Renart 2000; Renart et al. 2003). Therefore the fact that delay activity of prefrontal neurons in behaving monkeys indeed shows a high variability, as reported here, highlights a major inadequacy of the existing working memory models. Resolution of this issue will help to elucidate the microcircuit organization and dynamics of working memory cortical networks.

REFERENCES

Aertsen AMHJ, Gerstein GL, Habib MK, and Palm G. Dynamics of neuronal firing correlation: modulation of "effective connectivity." *J Neurophysiol* 61: 900–917, 1989.

Amit DJ and Brunel N. Model of global spontaneous activity and local structured activity during delay periods in the cerebral cortex. *Cereb Cortex* 7: 237–252, 1997.

Baddeley A. Working memory. *Science* 255: 556–559, 1992.

Baddeley R, Abbott LF, Booth MC, Sengpiel F, Freeman T, Wakeman EA, and Rolls ET. Responses of neurons in primary and inferior temporal visual cortices to natural scenes. *Proc R Soc Lond B Biol Sci* 22: 1775–1783, 1997.

Bair W, Koch C, Newsome WT, and Britten K. Power spectrum analysis of bursting cells in area MT in the behaving monkey. *J Neurosci* 14: 2870–2892, 1994.

Baker SN, Spinks R, Jackson A, and Lemon RN. Synchronization in monkey motor cortex during a precision grip task. I. Task-dependent modulation in single-unit synchrony. *J Neurophysiol* 85: 869–885, 2001.

Bringuier V, Fregnac Y, Baranyi A, Debanne D, and Shulz DE. Synaptic origin and stimulus dependency of neuronal oscillatory activity in the primary visual cortex of the cat. *J Physiol* 500: 751–774, 1997.

Brunel N. Dynamics of sparsely connected networks of excitatory and inhibitory spiking neurons. *J Comput Neurosci* 8: 183–208, 2000.

Brunel N and Wang X-J. Effects of neuromodulation in a cortical network model of object working memory dominated by recurrent inhibition. *J Comput Neurosci* 11: 63–85, 2001.

Brunel N and Wang X-J. What determines the frequency of fast network oscillations with irregular neural discharges? I. Synaptic dynamics and excitation-inhibition balance. *J Neurophysiol* 90: 415–430, 2003.

Camperi M and Wang X-J. A model of visuospatial working memory in prefrontal cortex: recurrent network and cellular bistability. *J Comput Neurosci* 5: 383–405, 1998.

Cardoso de Oliveira S, Thiele A, and Hoffmann KP. Synchronization of neuronal activity during stimulus expectation in a direction discrimination task. *J Neurosci* 17: 9248–9260, 1997.

Chafee MV and Goldman-Rakic PS. Matching patterns of activity in primate prefrontal area 8a and parietal area 7ip neurons during a spatial working memory task. *J Neurophysiol* 79: 2919–2940, 1998.

Compte A, Brunel N, Goldman-Rakic PS, and Wang X-J. Synaptic mechanisms and network dynamics underlying spatial working memory in a cortical network model. *Cereb Cortex* 10: 910–923, 2000.

Connors BW and Gutnick MJ. Intrinsic firing patterns of diverse neocortical neurons. *Trends Neurosci* 13: 99–104, 1990.

Constantinidis C, Franowicz MN, and Goldman-Rakic PS. Coding specificity in cortical microcircuits: a multiple electrode analysis of primate prefrontal cortex. *J Neurosci* 21: 3646–3655, 2001.

Constantinidis C and Goldman-Rakic PS. Correlated discharges among putative pyramidal neurons and interneurons in the primate prefrontal cortex. *J Neurophysiol* 88: 3487–3497, 2002.

Constantinidis C and Steinmetz MA. Neuronal activity in posterior parietal area 7a during the delay periods of a spatial memory task. *J Neurophysiol* 76: 1352–1355, 1996.

Courtney SM, Ungerleider LG, Keil K, and Haxby JV. Transient and sustained activity in a distributed neural system for human working memory. *Nature* 386: 608–611, 1997.

Crick F. *The Astonishing Hypothesis: The Scientific Search for the Soul.* New York: Charles Scribner's Sons, 1994.

Csicsvari J, Hirase H, Czurkó A, Mamiya A, and Buzsáki G. Oscillatory coupling of hippocampal cells and interneurons in the behaving rat. *J Neurosci* 19: 274–287, 1999.

Doiron B, Chacron MJ, Maler L, Longtin A, and Bastian J. Inhibitory feedback required for network oscillatory responses to communication but not prey stimuli. *Nature* 421: 539–543, 2003.

Durstewitz D, Seamans JK, and Sejnowski TJ. Dopamine-mediated stabilization of delay-period activity in a network model of prefrontal cortex. *J Neurophysiol* 83: 1733–1750, 2000.

Eckhorn R, Bauer R, Jordan W, Brosch M, Kruse W, Munk M, and Reitboeck HJ. Coherent oscillations: a mechanism of feature linking in the visual cortex? Multiple electrode and correlation analyses in the cat. *Biol Cybern* 60: 121–130, 1988.

Eckhorn R, Frien A, Bauer R, Woelbern T, and Kehr H. High frequency (60–90 Hz) oscillations in primary visual cortex of awake monkey. *Neuroreport* 4: 243–246, 1993.

Egorov AV, Hamam BN, Fransen E, Hasselmo ME, and Alonso AA. Graded persistent activity in entorhinal cortex neurons. *Nature* 420: 173–178, 2002.

Frank LM, Brown EN, and Wilson MA. A comparison of the firing properties of putative excitatory and inhibitory neurons from ca1 and the entorhinal cortex. *J Neurophysiol* 86: 2029–2040, 2001.

Friedman-Hill S, Maldonado PE, and Gray CM. Dynamics of striate cortical activity in the alert macaque. I. Incidence and stimulus-dependence of gamma-band neuronal oscillations. *Cereb Cortex* 10: 1105–1116, 2000.

Frien A, Eckhorn R, Bauer R, Woelburn T, and Kehr H. Stimulus-specific fast oscillations at zero phase between visual areas V1 and V2 of awake monkey. *Neuroreport* 5: 2273–2277, 1994.

Fries P, Reynolds JH, Rorie AE, and Desimone R. Modulation of oscillatory neuronal synchronization by selective visual attention. *Science* 291: 1560–1563, 2001.

Funahashi S, Bruce CJ, and Goldman-Rakic PS. Mnemonic coding of visual space in the monkey's dorsolateral prefrontal cortex. *J Neurophysiol* 61: 331–349, 1989.

Fuster JM and Alexander GE. Neuron activity related to short-term memory. *Science* 173: 652–654, 1971.

Gao W-J, Krimer LS, and Goldman-Rakic PS. Presynaptic regulation of recurrent excitation by D1 receptors in prefrontal circuits. *Proc Natl Acad Sci USA* 98: 295–300, 2001.

Ghose GM and Freeman RD. Oscillatory discharge in the visual system: does it have a functional role? *J Neurophysiol* 68: 1558–1574, 1992.

Goldman-Rakic PS. Circuitry of primate prefrontal cortex and regulation of behavior by representational memory. In: *Handbook of Physiology. The Nervous System. Higher Functions of the Brain.* Bethesda, MD: Am. Physiol. Soc, 1987, sect. 1, vol. V, chapt. 9, p. 373–417.

Goldman-Rakic PS. Cellular basis of working memory. *Neuron* 14: 477–485, 1995.

Gray CM, Konig P, Engel AK, and Singer W. Oscillatory responses in cat visual cortex exhibit inter-columnar synchronization which reflects global stimulus properties. *Nature* 338: 334–337, 1989.

Gray CM and McCormick DA. Chattering cells: superficial pyramidal neurons contributing to the generation of synchronous oscillations in the visual cortex. *Science* 274: 109–113, 1996.

Gray CM and Viana Di Prisco G. Stimulus-dependent neuronal oscillations and local synchronization in striate cortex of the alert cat. *J Neurosci* 17: 3239–3253, 1997.

Harwell M. Misinterpreting interaction effects in analysis of variance. *Measure Eval Counsel Dev* 32: 125–136, 1998.

Hempel CM, Hartman KH, Wang X-J, Turrigiano GG, and Nelson SB. Multiple forms of short-term plasticity at excitatory synapses in rat medial prefrontal cortex. *J Neurophysiol* 83: 3031–3041, 2000.

Holt GR, Softky WR, Koch C, and Douglas RJ. Comparison of discharge variability in vitro and in vivo in cat visual cortex neurons. *J Neurophysiol* 75: 1806–1814, 1996.

Jarvis MR and Mitra PP. Sampling properties of the spectrum and coherency of sequences of action potentials. *Neural Comput* 13: 717–749, 2001.

Jonides J, Smith EE, Koeppe RA, Awh E, Minoshima S, and Mintun MA. Spatial working memory in humans as revealed by PET. *Nature* 363: 623–625, 1993.

Judge SJ, Richmond BJ, and Chu FC. Implantation of magnetic search coils for measurement of eye position: an improved method. *Vision Res* 20: 535–538, 1980.

Kepecs A, Wang X-J, and Lisman J. Bursting neurons signal input slope. *J Neurosci* 22: 9053–9062, 2002.

Kiper DC, Gegenfurtner KR, and Movshon AJ. Cortical oscillatory responses do not affect visual segmentation. *Vision Res* 4: 539–544, 1996.

Kreiter AK and Singer W. Stimulus-dependent synchronization of neuronal responses in the visual cortex of the awake macaque monkey. *J Neurosci* 16: 2381–2396, 1996.

Kubota K and Niki H. Prefrontal cortical unit activity and delayed alternation performance in monkeys. *J Neurophysiol* 34: 337–347, 1971.

Leung H-C, Gore JC, and Goldman-Rakic PS. Sustained mnemonic response in the human middle frontal gyrus during on-line storage of spatial memoranda. *J Cogn Neurosci* 14: 659–671, 2002.

Lisman J. Bursts as a unit of neural information: making unreliable synapses reliable. *Trends Neurosci* 20: 38–43, 1997.

Lisman JE, Fellous JM, and Wang X-J. A role for NMDA-receptor channels in working memory. *Nat Neurosci* 1: 273–275, 1998.

Lisman JE and Idiart MAP. Storage of 7 ± 2 short-term memories in oscillatory subcycles. *Science* 267: 1512–1515, 1995.

Livingstone MS. Oscillatory firing and interneuronal correlations in squirrel monkey striate cortex. *J Neurophysiol* 75: 2467–2485, 1996.

Mardia KV, Kent JT, and Bibby JM. *Multivariate Analysis.* London: Academic Press, 1979.

McCarthy G, Blamire AM, Puce A, Nobre AC, Bloch G, Hyder F, Goldman-Rakic PS, and Shulman RG. Functional magnetic resonance imaging of human prefrontal cortex activation during a spatial working memory task. *Proc Natl Acad Sci USA* 91: 8690–8694, 1994.

Miller EK, Erickson CA, and Desimone R. Neural mechanisms of visual working memory in prefrontal cortex of the macaque. *J Neurosci* 16: 5154–5167, 1996.

Murthy VN and Fetz EE. Oscillatory activity in sensorimotor cortex of awake monkeys: synchronization of local field potentials and relation to behavior. *J Neurophysiol* 76: 3949–3967, 1996.

Nowak LG, Munk MH, Nelson JI, James AC, and Bullier J. Structural basis of cortical synchronization. I. Three types of interhemispheric coupling. *J Neurophysiol* 74: 2379–2400, 1995.

Nowak LG, Sanchez-Vives MV, and McCormick DA. Influence of low and high frequency inputs on spike timing in visual cortical neurons. *Cereb Cortex* 7: 487–501, 1997.

Pesaran B, Pezaris JS, Sahani M, Mitra PP, and Andersen RA. Temporal structure in neuronal activity during working memory in macaque parietal cortex. *Nat Neurosci* 5: 805–811, 2002.

Percival DB and Walden AT. *Spectral Analysis for Physical Applications: Multitaper and Conventional Univariate Techniques.* Cambridge, UK: Cambridge Univ. Press, 1993

Raghavachari S, Kahana MJ, Rizzuto DS, Caplan JB, Kirschen MP, Bourgeois B, Madsen JR, and Lisman JE. Gating of human theta oscillations by a working memory task. *J Neurosci* 21: 3175–3183, 2001.

Renart A. *Multi-modular Memory Systems* (PhD dissertation). Madrid, Spain: Universidad Autónoma de Madrid, 2000.

Renart A, Brunel N, and Wang X-J. Mean-field theory of recurrent cortical networks: working memory circuits with irregularly spiking neurons. In: *Computational Neuroscience: A Comprehensive Approach*, edited by Feng J. Boca Raton, FL: CRC Press, 2003.

Romo R, Brody CD, Hernandez A, and Lemus L. Neuronal correlates of parametric working memory in the prefrontal cortex. *Nature* 339: 470–473, 1999.

Sakai K, Rowe JB, and Passingham RE. Active maintenance in prefrontal area 46 creates distractor-resistant memory. *Nat Neurosci* 5: 479–484, 2002.

Sanes JN and Donoghue JP. Oscillations in local field potentials of the primate motor cortex during voluntary movement. *Proc Natl Acad Sci USA* 90: 4470–4474, 1993.

Schwarz C and Bolz J. Functional specificity of a long-range horizontal connection in cat visual cortex: a cross-correlation study. *J Neurosci* 11: 2995–3007, 1991.

Shadlen MN and Newsome WT. Noise, neural codes and cortical organization. *Curr Opin Neurobiol* 4: 569–579, 1994.

Shinomoto S, Sakai Y, and Funahashi S. The Ornstein-Uhlenbeck process does not reproduce spiking statistics of neurons in prefrontal cortex. *Neural Comput* 11: 935–951, 1999.

Shu Y, Hasenstaub A, and McCormick DA. Turning on and off recurrent balanced cortical activity. *Nature* 423: 288–293, 2003.

Singer W and Gray CM. Visual feature integration and the temporal correlation hypothesis. *Annu Rev Neurosci* 18: 555–586, 1995.

Softky WR and Koch C. The highly irregular firing of cortical cells is inconsistent with temporal integration of random EPSPs. *J Neurosci* 13: 334–350, 1993.

Tallon-Baudry C, Bertrand O, and Fischer C. Oscillatory synchrony between human extrastriate areas during visual short-term memory maintenance. *J Neurosci* 21: RC177, 2001.

Tegnér J, Compte A, and Wang X-J. The dynamical stability of reverberatory neural circuits. *Biol Cybern* 87: 471–481, 2002.

Tenenbaum JB, de Silva V, and Langford JC. A global geometric framework for nonlinear dimensionality reduction. *Science* 290: 2319–2323, 2000.

Thomson DJ and Chave AD. Jackknifed error estimates for spectra, coherences, and transfer functions. In: *Advances in Spectrum Analysis and Array Processing*, edited by Haykin S. Englewood Cliffs, NJ: Prentice-Hall, 1991, p. 58–113.

Tovee MJ and Rolls ET. Oscillatory activity is not evident in the primate temporal visual cortex with static stimuli. *Neuroreport* 3: 369–372, 1992.

Treisman AM. The binding problem. *Curr Opin Neurobiol* 6: 171–178, 1996.

Troyer T and Miller KD. Physiological gain leads to high ISI variability in a simple model of a cortical regular spiking cell. *Neural Comput* 9: 971–983, 1997.

van Vreeswijk C and Sompolinsky H. Chaotic balanced state in a model of cortical circuits. *Neural Comput* 10: 1321–1371, 1998.

Wang X-J. Fast burst firing and short-term synaptic plasticity: a model of neocortical chattering neurons. *Neuroscience* 89: 347–362, 1999a.

Wang X-J. Synaptic basis of cortical persistent activity: the importance of NMDA receptors to working memory. *J Neurosci* 19: 9587–9603, 1999b.

Wang X-J. Synaptic reverberation underlying mnemonic persistent activity. *Trends Neurosci* 24: 455–463, 2001.

Wilbur WJ and Rinzel J. A theoretical basis for large coefficient of variation and bimodality in neuronal interspike interval distributions. *J Theor Biol* 105: 345–368, 1983.

Young MP, Tanaka K, and Yamane S. On oscillating neuronal responses in the visual cortex of the monkey. *J Neurophysiol* 67: 1464–1474, 1992.